AIP | Journal of Applied Physics

Equivalent circuit model for organic single-layer diodes

A. Haldi, A. Sharma, W. J. Potscavage, and B. Kippelen

Citation: J. Appl. Phys. **104**, 064503 (2008); doi: 10.1063/1.2980324
View online: http://dx.doi.org/10.1063/1.2980324
View Table of Contents: http://jap.aip.org/resource/1/JAPIAU/v104/i6
Published by the American Institute of Physics.

Equivalent circuit model for organic single-layer diodes

A. Haldi, A. Sharma, W. J. Potscavage, Jr., and B. Kippelen[a)]
Center for Organic Photonics and Electronics (COPE), School of Electrical and Computer Engineering, Georgia Institute of Technology, Atlanta, Georgia 30332, USA

(Received 8 April 2008; accepted 22 July 2008; published online 19 September 2008)

A simple equivalent circuit is proposed to model single-layer organic diodes. The circuit is based on thermionic emission to describe carrier injection from the electrode into the organic semiconductor and on space-charge limited currents across the semiconductor. By fitting the electrical characteristics measured as a function of temperature with the model, intrinsic material and interface parameters such as the mobility and the injection barrier energy are extracted. The resulting parameters agree well with independently measured values in the literature. © *2008 American Institute of Physics*. [DOI: 10.1063/1.2980324]

I. INTRODUCTION

In recent years, organic semiconductors have been incorporated into a variety of solid-state devices such as organic light-emitting devices (OLEDs), organic solar cells, organic diodes, and organic field-effect transistors.[1–4] When integrating these devices in circuits that have increasing complexity, it becomes critical to have accurate and relatively simple models to describe their electrical characteristics. For instance, OLEDs are often modeled with a single diode equation but the predictive capabilities of this oversimplified model in describing the electrical properties over the full range of voltages are rather limited.

Different approaches to model organic diodes have been reported in the literature. Simple models are achieved with partial fits of the electrical characteristics in the low voltage or in the high voltage range. For example, the steep increase in current at low voltages has mostly been attributed to thermionic or Schottky emission of charges across the energy barrier between the Fermi level of the electrode and the highest occupied molecular orbital (HOMO) or the lowest unoccupied molecular orbital (LUMO) of the organic layer.[5,6]

The current at higher voltages is usually assumed to be limited by space-charge limited current (SCLC) effects.[7–9] However, besides for materials that make almost Ohmic contact [i.e., indium tin oxide (ITO)/poly(2-methoxy,5-(2′ethyl-hexyloxy)-*p*-phenylene vinylene) (MEH-PPV)], the electrical characteristics mostly follow a power law with an exponent that is substantially larger than 2.[10,11] In general, simple models that consist of just one circuit element cannot fit the full electrical characteristics and are limited to partial fits in selected regions of the current-voltage characteristics.

Alternatively, better fits of the electrical characteristics have been achieved using more complex models based on basic semiconductor and electromagnetic equations.[12–14] These systems of equations are usually solved in a finite element approach where the carrier and field distributions inside an organic layer are calculated and optimized to fit given boundary conditions. Although such calculations can lead to quite accurate fits of experimental data, they are heavily dependent on parameters such as the intrinsic charge carrier density or the intrinsic electric field that cannot be measured in an independent experiment, and a wide range of values has been published for these parameters.[12,15–17] Furthermore, such complicated systems of equations cannot be easily integrated in circuit design software for accurate modeling of organic devices.

In this paper, we present an equivalent circuit approach to model the electrical characteristics of a basic organic single-layer diode that is implemented in SPICE, a widely used circuit-simulation program. The equivalent circuit model is based on physical principles of an organic diode and will be explained in Sec. II. Then, temperature-dependent experimental electrical characteristics of different single-layer diodes will be fitted with the proposed model to extract material parameters. Finally, the resulting parameters will be compared to the material parameters that are reported in the literature.

II. THEORY AND MODEL

The injection of a charge into an organic semiconductor is generally considered to be based on thermionic emission across the energy barrier that is formed between the work function of the injecting electrode and the HOMO or LUMO of the organic semiconductor depending on whether hole or electron injection, respectively, is considered. The current density J across this energy barrier can be modeled using the general diode equation

$$J = J_0\left(\exp\left[\frac{qV}{nkT}\right] - 1\right), \tag{1}$$

where J_0 is the saturation current density, q is the elementary charge, V is the applied voltage, n is the ideality factor, k is the Boltzmann constant, and T is the temperature. For thermionic emission, the saturation current density J_0 is given by the equation

[a)]Author to whom correspondence should be addressed. Electronic mail: kippelen@ece.gatech.edu.

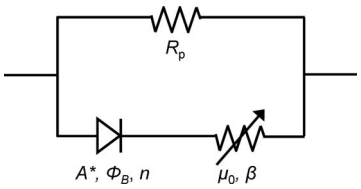

FIG. 1. Equivalent circuit of an organic single-layer diode.

$$J_0 = A^* T^2 \exp\left(-\frac{\Phi_B}{kT}\right), \tag{2}$$

where A^* is the Richardson constant and Φ_B is the injection barrier for charges.[18]

Once the charges have been injected, they have to travel across the organic semiconductor to the opposite electrode. It has been shown for organic materials that this drift current is a SCLC and follows the equation

$$J = \frac{9}{8}\mu\varepsilon\varepsilon_0\frac{V^2}{L^3}, \tag{3}$$

where μ is the mobility, ε the dielectric constant, ε_0 the permittivity of free space, and L the thickness of the sample.[19] Furthermore, based on the framework of the disorder formalism,[20,21] the mobility in an organic material is given by

$$\mu = \mu_{0,0} \exp\left[-\left(\frac{2\sigma}{3k_B T}\right)^2\right]\exp\left[\beta\sqrt{\frac{V}{L}}\right], \tag{4}$$

where $\mu_{0,0}$ is the mobility at zero field and zero temperature, σ is the width of the energetical disorder distribution, and β is the field-dependence factor of the mobility. Since $\mu_{0,0}$ and σ cannot be determined independently in a measurement where only the applied voltage is varied, a simplified version of Eq. (4) is used in our model:

$$\mu = \mu_0(T)\exp\left(\beta\sqrt{\frac{V}{L}}\right), \tag{5}$$

with $\mu_0(T)$ the temperature-dependent zero-field mobility.

Based on these physical observations, an equivalent circuit model for an organic single-layer diode is proposed that consists of a diode for injection into the organic semiconductor, in series with a voltage-dependent resistor representing the SCLC for the bulk conductivity in the device (Fig. 1). A shunt resistor R_p is placed in parallel to these two circuit elements to account for any leakage current through the device.

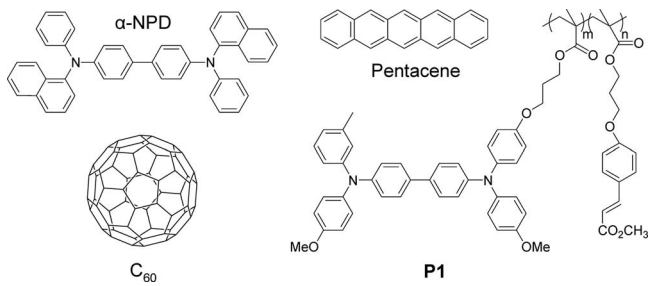

FIG. 2. Chemical structure of α-NPD, P1 (with $m:n=8:2$), C_{60}, and pentacene.

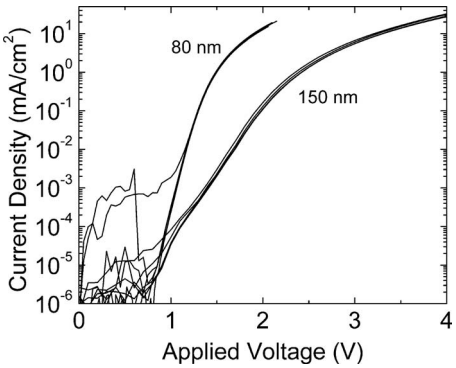

FIG. 3. Current density vs applied voltage at room temperature for α-NPD diodes with thicknesses of 80 and 150 nm. Plots of five devices are overlapped for each thickness.

III. EXPERIMENT

Four different materials were used as the organic layer in a single-layer device geometry (see Fig. 2). 4,4′-bis[*N*-(1-naphthyl)-*N*-phenyl-amino]biphenyl (α-NPD) and *N*,*N*′-bis(*m*-tolyl)-*N*,*N*′-diphenyl-1,1′-biphenyl-4,4′-diamine (TPD) are well-known hole-transport materials with a wide bandgap.[22,23] Whereas α-NPD was used in its small molecule form, a TPD-based polymer[24] (P1) was used for another set of devices to make sure that the proposed model applies not only to small molecule but also to polymers. Other devices incorporated a layer of the electron-transport organic semiconductor C_{60} or a layer of the hole-transport material pentacene. These latter two materials were selected because they have a significantly higher mobility[4,25] and a smaller bandgap[2] compared to α-NPD and P1.

Diodes were fabricated on air plasma treated ITO coated glass substrates with a sheet resistance of 20 $\Omega/\square$ (Colorado Concept Coatings, L.L.C.). For the organic layer, the small molecules of C_{60} and pentacene were purified using gradient zone sublimation. The films consisting of small molecules were then thermally evaporated at a pressure below 1×10^{-7} Torr on top of ITO. For C_{60} diodes, an additional layer of 8 nm bathocuproine (2,9-dimethyl-4,7-diphenyl-1,10-phenanthroline, BCP) was deposited on top of the fullerenes to avoid aluminum diffusion into the C_{60}.[26]

For the polymer diode, a 90 nm thick film was spin coated from toluene on top of the air plasma treated ITO substrates. The films were crosslinked using a standard broad-band UV light with a 0.7 mW/cm^2 power density for 1 min. For all diodes, a 200 nm thick aluminum cathode was vacuum deposited on top of the organic layer at a pressure below 1×10^{-6} Torr and at a rate of 2 Å/s. A shadow mask was used for the evaporation of the metal to form five devices with an area of 0.1 cm^2 per substrate. At no point during device fabrication and testing were the devices exposed to atmospheric conditions. Finally, model parameter values were determined by fitting the experimental data with the equivalent circuit model using the HSPICE optimization tool.

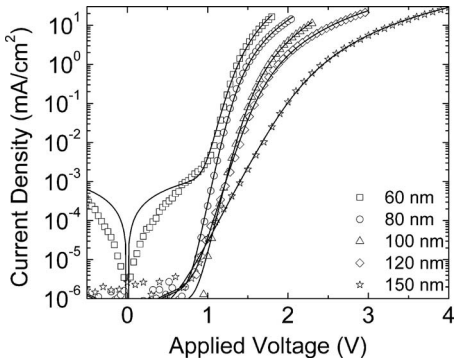

FIG. 4. Current density vs applied voltage at room temperature for α-NPD diodes with thicknesses ranging from 60 to 150 nm. Experimental data are shown as empty symbols; solid lines represent the simulated curves.

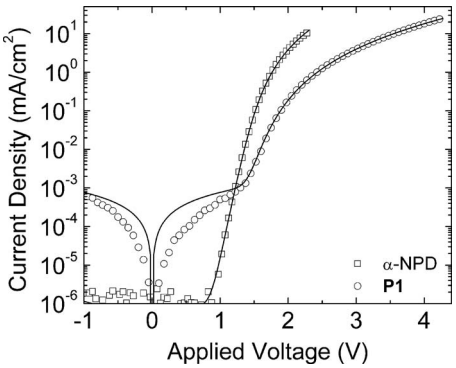

FIG. 5. Current density vs applied voltage at room temperature for organic diodes with organic layers of α-NPD (100 nm, squares) and P1 (90 nm, circles). Experimental data are shown as empty symbols; solid lines represent the simulated curves.

IV. RESULTS AND DISCUSSION

When testing a model it is important to verify that the experimental electrical characteristics to which the model is applied are highly reproducible. Figure 3 shows the data of five different devices with the ITO/α-NPD (80 nm)/Al geometry and five different devices with the ITO/α-NPD (150 nm)/Al geometry. The high reproducibility of these electrical characteristics lead to an error of less than 10% of the fitted values for the ideality factor n and the zero-field mobility μ_0. For the saturation current density J_0 and the field dependence of the mobility β, the error is higher and can reach $\pm 100\%$ of the fitted value.

In the next step, to test the validity of the SCLC, α-NPD diodes with different thicknesses were fabricated and tested. Model parameters were extracted from fits to the experimental data (see Fig. 4) and are summarized in Table I. The mobility parameters are found to be nearly independent of the thickness, which supports the introduction of the SCLC voltage-dependent series resistor in our model.

Likewise, the model was applied to the experimental data of diodes with the ITO/P1 (90 nm)/Al geometry, and good fits were obtained except for the low voltage range (Fig. 5). In our model, the current in that region is dominated by the parallel resistor R_p, even though the experimental data do not show a linear increase. However, since diodes, especially OLEDs, are operated at higher voltages where current injection is more efficient, a certain discrepancy of the equivalent circuit at low voltages does not seem to be very problematic.

From the electrical characteristics of the α-NPD diodes and the diodes of P1 at room temperature, the mobility values were determined as 1.2×10^{-4} and 4.5×10^{-6} cm^2/V s, respectively (see Table II). These values are in good agreement with mobility values measured in time-of-flight experiments and SCLC measurements.[27–29] Furthermore, the temperature dependence of the mobility can be determined from measurements of the organic single-layer diode at different temperatures, as shown in Fig. 6 for a device with the ITO/α-NPD (100 nm)/Al geometry, where the four parameters J_0, n, μ_0, and β were extracted separately at each temperature. Combining Eqs. (4) and (5), the mobility at zero field and zero temperature $\mu_{0,0}$ as well as the width of the energetical disorder distribution σ can be calculated from the intercept and the slope, respectively, of a linear fit when plotting the logarithm of the zero-field mobility μ_0 versus T^2. In fact, such plots of our extracted parameters resulted in reasonable fits for the α-NPD diodes and the diodes incorporating P1 (Fig. 7). The widths of the energetical disorder distribution σ was calculated to be 0.096 and 0.128 eV for diodes incorporating α-NPD and P1, respectively. The corresponding zero-field and zero-temperature mobility values were $\mu_{0,0}=7.0\times10^{-2}$ cm^2/V s for α-NPD and $\mu_{0,0}=3.8\times10^{-1}$ cm^2/V s for P1.

Despite the good agreement of the proposed model for the previous diodes, some adjustments to the equivalent circuit were necessary to fit the electrical characteristics of diodes based on pentacene and C_{60}. Typically, organic semiconductors show Ohmic behavior before SCLC occurs. Combining Eq. (3) with the equation for Ohmic drift current,

TABLE I. Saturation current density J_0, ideality factor n, parallel resistance R_p, zero-field mobility μ_0, and mobility field-dependence factor β, all extracted from electrical characteristics at room temperature for α-NPD diodes with different thicknesses L.

L (nm)	J_0 (mA/cm^2)	n	R_p (Ω cm^2)	μ_0 (cm^2/V s)	β [(cm/V)$^{1/2}$]
60	1.1×10^{-11}	2.0	8.0×10^{5}	1.8×10^{-4}	1.1×10^{-6}
80	6.2×10^{-14}	1.7	4.1×10^{8}	1.5×10^{-4}	4.9×10^{-6}
100	1.8×10^{-14}	1.9	8.7×10^{8}	1.2×10^{-4}	1.5×10^{-3}
120	6.5×10^{-12}	2.5	3.8×10^{8}	1.8×10^{-4}	1.0×10^{-7}
150	3.5×10^{-9}	4.3	9.8×10^{8}	2.4×10^{-4}	1.2×10^{-4}

TABLE II. Saturation current density J_0, ideality factor n, parallel resistance R_p, zero-field mobility μ_0, and mobility field-dependence factor β, all extracted from electrical characteristics at room temperature for organic diodes with thickness L. For pentacene and C_{60}, the series resistance R_s is noted instead of any mobility. The Richardson constant A^* and the injection barrier Φ_B were extrapolated from measurements at different temperatures.

	L (nm)	J_0 (mA/cm^2)	n	R_p (Ω cm^2)	μ_0 (cm^2/V s)	β [(cm/V)$^{1/2}$]	R_s (Ω cm^2)	A (A/cm^2 K^2)	Φ_B (eV s)
α-NPD	100	1.8×10^{-14}	1.9	8.7×10^{8}	1.2×10^{-4}	1.5×10^{-3}	N/A	1.9×10^{-5}	0.99
P1	90	1.5×10^{-14}	2.2	1.3×10^{6}	4.5×10^{-6}	2.8×10^{-3}	N/A	⋯	⋯
Pentacene	80	7.7×10^{-4}	1.6	1.7×10^{6}	N/A	N/A	1.4	1.2×10^{-4}	0.42
C_{60}	100	3.6×10^{-9}	1.7	2.7×10^{4}	N/A	N/A	1.1	1.8×10^{-5}	0.72

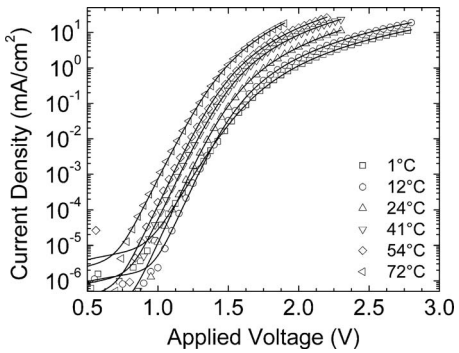

FIG. 6. Current density vs applied voltage for an α-NPD diode with a thickness of 100 nm measured at temperatures ranging from 1 to 72 °C. Experimental data are shown as empty symbols; solid lines represent the simulated curves.

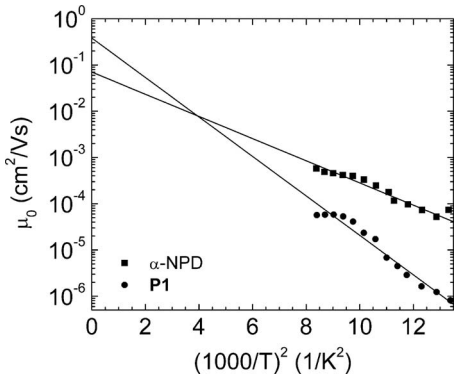

FIG. 7. Plot of zero-field mobility vs $(1000/T)^2$ for organic diodes consisting of α-NPD (100 nm, squares) and P1 (90 nm, circles). Experimental data are shown as empty symbols; solid lines are linear fits to this data.

$$J = n_0 e \mu \frac{V}{L}, \tag{6}$$

where e is the elementary charge and n_0 the charge carrier density, a crossover voltage V_C from Ohmic to SCLC can be calculated yielding

$$V_C = \frac{8}{9}\frac{e}{\varepsilon}L^2 n_0, \tag{7}$$

with

$$n_0 \propto \exp\left(-\frac{E_g}{2kT}\right), \tag{8}$$

where E_g is the bandgap of the material. From Eq. (7), it can be seen that the crossover voltage between the Ohmic and SCLC regimes is increased when using materials with smaller bandgaps such as pentacene and C_{60}. Hence, Ohmic (linear) drift current can still be observed even at high voltages in diodes based on pentacene or C_{60} (E_g: 1.9 and 1.7 eV, for pentacene and C_{60},[2] respectively) compared to α-NPD or TPD [E_g: 3.1 and 3.2 eV for α-NPD (Ref. 30) and TPD,[6] respectively]. In fact, by replacing the SCLC resistor in our model with a constant resistor R_s, good fits to the experimental data of pentacene and C_{60} diodes can be achieved (see Fig. 8), which has already been shown in equivalent circuits of pentacene/C_{60} organic photovoltaic cells. However, no mobility values can be determined from R_s since both the charge carrier concentration n_0 and the mobility μ are unknown in the equation for R_s:

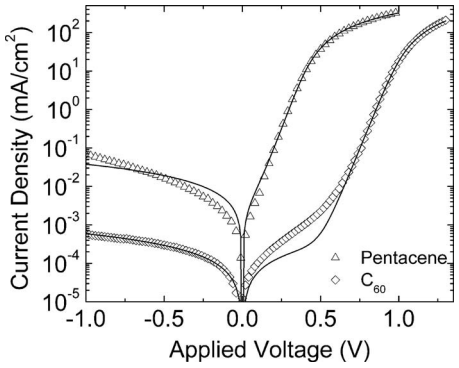

FIG. 8. Current density v applied voltage at room temperature for organic diodes with organic layers of pentacene (80 nm, triangles) and C_{60}/BCP (100 nm/8 nm, diamonds). Experimental data are shown as empty symbols; solid lines represent the simulated curves.

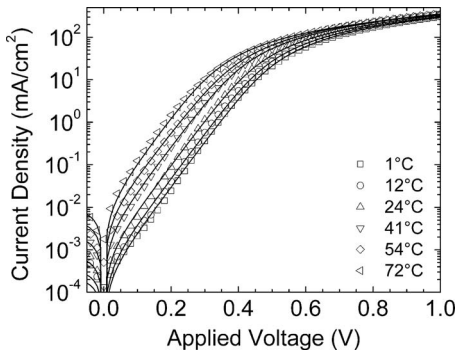

FIG. 9. Current density vs applied voltage for a pentacene diode with a thickness of 80 nm measured at temperatures ranging from 1 to 72 °C. Experimental data are shown as empty symbols; solid lines represent the simulated curves.

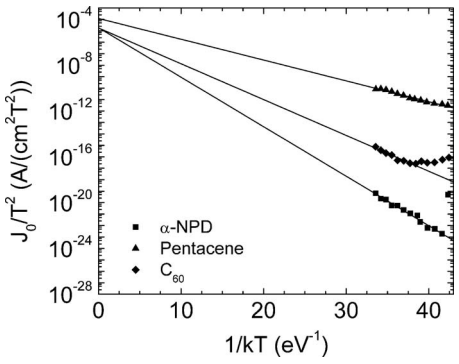

FIG. 10. Plot of (J_0/T^2) vs $(1/kT)$ for organic diodes consisting of three different materials to extrapolate the injection barrier Φ_B and the Richardson constant A^*. Experimental data are shown as empty symbols; solid lines are linear fits to the data.

$$R_s = \frac{L}{n_0 e \mu}. \tag{9}$$

Finally, to calculate the injection barrier and the Richardson constant, current density measurements in single-layer diodes were performed as a function of temperature (see Fig. 6 for α-NPD and Fig. 9 for pentacene diodes). By plotting the logarithm of (J_0/T^2) versus $(1/kT)$, the injection barrier and the Richardson constant can be determined from the slope and the intercept, respectively, in a linear fit of the experimental data as a function of temperature, as shown in Fig. 10. Calculated values of the fitted parameters are summarized in Table II. Note that data from diodes incorporating P1 did not yield a linear fit. Hence, the values of the Richardson constant and the injection barrier energy could not be extracted. Furthermore, deviations between the model and the data were observed at the lowest temperatures in diodes with C_{60}. The origin of these deviations is currently under investigation.

All calculated Richardson constants were in the range of 10^{-5}–10^{-4} A/cm^2 K^2, which is in the upper range of experimentally determined Richardson constants in organic materials[6,31,32] but below the theoretical value of $\sim 10^{-2}$ A/cm^2 K^2.[33] The fitted injection barrier for the C_{60} diodes (Φ_B=0.72 eV) seems to suggest that electrons are in fact not injected from the aluminum (work function W =4.2 eV) into the C_{60} film (LUMO: 4.5 eV)[2] through defect states in the BCP, as was mentioned in earlier reports.[34] More likely, electrons get injected into the LUMO of BCP since the measured injection barrier corresponds well with the barrier between aluminum and BCP (LUMO of BCP: 3.5 eV).[2]

In the case of the α-NPD and the pentacene diodes, both values for the injection barriers that were calculated from the fits in Fig. 9 are higher than the energy barriers that are expected between the work function of plasma treated ITO (W=4.7 eV) (Ref. 35) and the HOMO energies of α-NPD (5.5 eV) (Ref. 30) and of pentacene (4.9 eV).[2] However, similar values for the energy barrier have resulted from x-ray photoemission spectroscopy and ultraviolet photoemission spectroscopy (UPS) measurements,[36,37] and the increased barrier energies have been attributed to dipoles that form at the interface to ITO, which causes a vacuum level mialignment and therefore an increase in the injection barrier.

V. SUMMARY

In conclusion, an equivalent circuit model for organic diodes is proposed. The model assumes that injection of charges from an electrode into the organic semiconductor is governed by thermionic emission. The drift current across the semiconductor is then described by a voltage-dependent resistor representing SCLC in series with the injecting diode.

Applying this model to the experimental data of two single-layer diodes consisting of α-NPD and a TPD-based polymer P1 returned mobilities that are similar to published results. Furthermore, the extracted values are consistent with the disorder formalism of the mobility, which was confirmed by temperature-dependent measurements of the electrical characteristics.

For pentacene and C_{60} diodes, the equivalent circuit had to be modified by replacing the voltage-dependent resistor with a constant resistor to represent the Ohmic drift current that can be observed in such diodes due to the small bandgap of the two materials. No information about the mobility values could be gained from this model since the current within the considered voltage range did not reach the SCLC regime in the devices with lower bandgap materials.

Finally, Richardson constants and injection barrier energies could also be extracted from temperature dependence measurements of the electrical characteristics of the diodes. Both parameters were in good agreement with measured parameters in the literature.

Combining these results, it has been shown that the proposed equivalent circuit is a simple but reliable model to simulate organic single-layer diodes. The model is mainly based on parameters that can be extracted from independent experiments, such as mobility or UPS measurements. With the implementation of the equivalent circuit in SPICE, the model can also be readily used in circuit optimizations. However, it has to be noted that the proposed model at this stage does not fit well for high-efficiency OLEDs composed of multiple layers and that further refinements to the current model will be required.

ACKNOWLEDGMENTS

This material is based upon work supported in part by the STC Program of the National Science Foundation under Agreement No. DMR-0120967 and by the Office of Naval Research through a MURI program. The authors would like to thank Dr. B. Domercq for helpful discussions and Professor S. R. Marder and his group from the School of Chemistry and Biochemistry for providing the P1 polymer.

[1] M. A. Baldo, S. Lamansky, P. E. Burrows, M. E. Thompson, and S. R. Forrest, Appl. Phys. Lett. **75**, 4 (1999).
[2] S. Yoo, B. Domercq, and B. Kippelen, Appl. Phys. Lett. **85**, 5427 (2004).
[3] S. Steudel, K. Myny, V. Arkhipov, C. Deibel, S. De Vusser, J. Genoe, and P. Heremans, Nat. Mater. **4**, 597 (2005).
[4] S. F. Nelson, Y. Y. Lin, D. J. Gundlach, and T. N. Jackson, Appl. Phys. Lett. **72**, 1854 (1998).
[5] K. Harada, A. G. Werner, M. Pfeiffer, C. J. Bloom, C. M. Elliott, and K. Leo, Phys. Rev. Lett. **94**, 036601 (2005).
[6] A. J. Campbell, D. D. C. Bradley, J. Laubender, and M. Sokolowski, J. Appl. Phys. **86**, 5004 (1999).
[7] L. Bozano, S. A. Carter, J. C. Scott, G. G. Malliaras, and P. J. Brock, Appl. Phys. Lett. **74**, 1132 (1999).

[8]G. G. Malliaras and J. C. Scott, J. Appl. Phys. **85**, 7426 (1999).
[9]A. Kumar, P. K. Bhatnagar, P. C. Mathur, M. Husain, S. Sengupta, and J. Kumar, J. Appl. Phys. **98**, 024502 (2005).
[10]P. W. M. Blom, M. J. M. deJong, and J. J. M. Vleggaar, Appl. Phys. Lett. **68**, 3308 (1996).
[11]W. Brutting, S. Berleb, and A. G. Muckl, Synth. Met. **122**, 99 (2001).
[12]P. S. Davids, I. H. Campbell, and D. L. Smith, J. Appl. Phys. **82**, 6319 (1997).
[13]C. C. Lee, Y. D. Jong, P. T. Huang, Y. C. Chen, P. J. Hu, and Y. Chang, Jpn. J. Appl. Phys., Part 1 **44**, 8147 (2005).
[14]F. Neumann, Y. A. Genenko, C. Melzer, and H. von Seggern, J. Appl. Phys. **100**, 084511 (2006).
[15]I. Kamohara, M. Townsend, and B. Cottle, J. Appl. Phys. **97**, 014501 (2005).
[16]S. J. Martin, A. B. Walker, A. J. Campbell, and D. D. C. Bradley, J. Appl. Phys. **98**, 063709 (2005).
[17]T. Ogawa, D.-C. Cho, K. Kaneko, T. Mori, and T. Mizutani, Thin Solid Films **438–439**, 171 (2003).
[18]R. F. Pierret, *Semiconductor Device Fundamentals*, 2nd ed. (Addison-Wesley, Reading, MA, 1996).
[19]M. A. Lampert and P. Mark, *Current Injection in Solids* (Academic, New York, 1970).
[20]H. Bassler, Phys. Status Solidi B **175**, 15 (1993).
[21]P. M. Borsenberger, L. Pautmeier, and H. Bassler, J. Chem. Phys. **94**, 5447 (1991).
[22]S. T. Zhang, Z. J. Wang, J. M. Zhao, Y. Q. Zhan, Y. Wu, Y. C. Zhou, X. M. Ding, and X. Y. Hou, Appl. Phys. Lett. **84**, 2916 (2004).
[23]J. L. Maldonado, M. Bishop, C. Fuentes-Hernandez, P. Caron, B. Domercq, Y. D. Zhang, S. Barlow, S. Thayumanavan, M. Malagoli, J. L. Bredas, S. R. Marder, and B. Kippelen, Chem. Mater. **15**, 994 (2003).
[24]B. Domercq, R. D. Hreha, Y. D. Zhang, N. Larribeau, J. N. Haddock, C. Schultz, S. R. Marder, and B. Kippelen, Chem. Mater. **15**, 1491 (2003).
[25]N. J. Haddock, B. Domercq, and B. Kippelen, Electron. Lett. **41**, 444 (2005).
[26]P. Peumans, A. Yakimov, and S. R. Forrest, J. Appl. Phys. **93**, 3693 (2003).
[27]S. Naka, H. Okada, H. Onnagawa, Y. Yamaguchi, and T. Tsutsui, Synth. Met. **111–112**, 331 (2000).
[28]T. Y. Chu and O. K. Song, Appl. Phys. Lett. **90**, 203512 (2007).
[29]B. Domercq, R. D. Hreha, Y. D. Zhang, A. Haldi, S. Barlow, S. R. Marder, and B. Kippelen, J. Polym. Sci., Part B: Polym. Phys. **41**, 2726 (2003).
[30]V. I. Adamovich, S. R. Cordero, P. I. Djurovich, A. Tamayo, M. E. Thompson, B. W. D'Andrade, and S. R. Forrest, Org. Electron. **4**, 77 (2003).
[31]S. Barth, P. Muller, H. Riel, P. F. Seidler, W. Rie, H. Vestweber, U. Wolf, and H. Bassler, Synth. Met. **111–112**, 327 (2000).
[32]F. Yakuphanoglu, E. Basaran, B. F. Senkal, and E. Sezer, J. Phys. Chem. B **110**, 16908 (2006).
[33]J. C. Scott and G. G. Malliaras, Chem. Phys. Lett. **299**, 115 (1999).
[34]P. Peumans and S. R. Forrest, Appl. Phys. Lett. **79**, 126 (2001).
[35]D. J. Milliron, I. G. Hill, C. Shen, A. Kahn, and J. Schwartz, J. Appl. Phys. **87**, 572 (2000).
[36]I. G. Hill and A. Kahn, J. Appl. Phys. **86**, 2116 (1999).
[37]N. J. Watkins, L. Yan, and Y. L. Gao, Appl. Phys. Lett. **80**, 4384 (2002).